ChemPhotoChem

Minireviews
doi.org/10.1002/cptc.202100143

Chemistry Europe
European Chemical Societies Publishing

www.chemphotochem.org

Special Collection

Lanthanide-Based Complexes Containing a Chiral *trans*-1,2-Diaminocyclohexane (DACH) Backbone: Spectroscopic Properties and Potential Applications

Fabio Piccinelli,*[a] Chiara Nardon,[a] Marco Bettinelli,[a] Andrea Melchior,*[b] Marilena Tolazzi,[b] Francesco Zinna,[c] and Lorenzo Di Bari*[c]

In this minireview, we give an overview on the use of the chiral molecule *trans*-1,2-diaminocyclohexane (DACH) in several fields of application. This chiral backbone is present in a variety of metal complexes which are employed in (enantioselective) catalysis, chiral discrimination, molecular recognition and supramolecular chemistry. Metal extraction and biochemical and pharmaceutical applications also use the DACH molecule. This contribution is particularly focused on the interesting chemical-physical properties discussed so far in the literature concerning lanthanide-based complexes containing chiral ligands characterized by the presence of DACH in the structure. In particular, the interconnection between luminescence (total and circularly polarized), structure and thermodynamics of Eu(III), Tb(III) and Sm(III) complexes will be discussed also in light of their use as optical or chiroptical probes for the sensing of important analytes dissolved in aprotic and protic polar solvents. Several complexes show potential interest in the solid state as phosphors for light emitting devices or for the detection of volatile organic compounds.

1. Introduction

DACH – *trans*-1,2-diaminocyclohexane, also known as *trans*-cyclohexane-1,2-diamine (CHDA or Chxn, Figure 1) – is an organic compound with molecular formula $C_6H_{14}N_2$ (MW = 114.19) and a key role in many fields, spanning from catalysis, material science and technology to the pharmaceutical area.

It is commercially available and can be obtained by hydrogenation of *o*-phenylenediamine or 1,2-dinitrocyclohexane. An improved method for the racemic resolution of the *trans* enantiomers has been proposed by H.-J. Schanz et al.[1] The chiral nature of DACH, associated with the two enantiomers (1R,2R)-DACH and (1S,2S)-DACH, is broadly exploited as a building block during ligand/scaffold designing prior to solution chemistry. Before leaping into the main subject of this review, that can be inferred from the title, we would like to give the reader a snapshot of the successful application involving this chiral molecule.

[a] *Prof. F. Piccinelli, Dr. C. Nardon, Prof. M. Bettinelli*
Luminescent Materials Laboratory
DB, University of Verona, and INSTM, UdR Verona
Strada Le Grazie 15, 37134 Verona (Italy)
E-mail: fabio.piccinelli@univr.it
[b] *Prof. A. Melchior, Prof. M. Tolazzi*
Dipartimento Politecnico di ingegneria e architettura
Laboratorio di Tecnologie Chimiche, University of Udine
Via Cotonificio 108, 33100 Udine (Italy)
E-mail: andrea.melchior@uniud.it
[c] *Dr. F. Zinna, Prof. L. Di Bari*
Department of Chemistry and Industrial Chemistry
Via Moruzzi 13, 56124 Pisa (Italy)
E-mail: lorenzo.dibari@unipi.it

Special Collection An invited contribution to a Special Collection on Circularly Polarized Luminescence.

1.1. DACH in Catalysis

Very recent examples underline the key role of such a chiral fragment in achieving astonishing enantioselectivity in catalytic reactions. Complexes of Pd (compound **I**, Figure 2) are capable to perform allenylation of pyrazolone[2] and the synthesis of quaternary α-allyl amino acids, as in the case of the Trost ligand (compound **II**, Figure 2)[3] with very high yield and enantiomeric excess (*ee*).

Similarly, S. H. Bergens and co-workers[4] exploited the 1R,2R enantiomer and reported the first highly enantioselective hydrogenation of racemic acyclic esters to β-chiral primary alcohols via dynamic kinetic resolution (DKR). The new ruthenium-based catalytic system recorded up to 1000 turnovers, 100% conversion and 95% enantiomeric excess (compound **III**, Figure 2). Among the *salen*-like ligands, those involving the condensation of two equivalents of salicylaldehyde (or analogues) with one of enantiomerically pure DACH are important not only in asymmetric catalysis but also in several current applications,[5–8] including environmental pro-

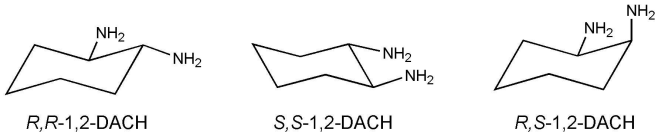

R,R-1,2-DACH *S,S*-1,2-DACH *R,S*-1,2-DACH

Figure 1. Chemical structure of DACH – *trans*-1,2-diaminocyclohexane (both R,R and S,S-1,2-DACH enantiomers) and DACH – *cis*-1,2-diaminocyclohexane (*meso* achiral isomer).

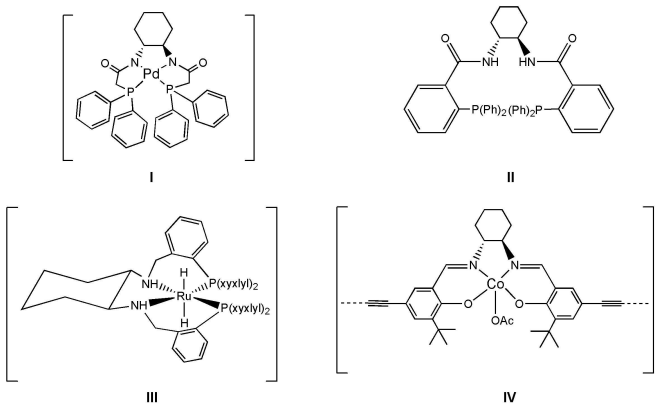

Figure 2. Chemical structure of the DACH-based catalytic complexes discussed in the text.

tection – subject more relevant than ever. For example, with the goal of combining the CO_2 capture with its transformation into high-added value compounds through catalytic reactions, Chun and co-workers prepared microporous organic networks (MONs) bearing a Cobalt-salen complex (compound **IV**, Figure 2) capable to efficiently fix CO_2 and to promote its conversion into cyclic carbonates.[9] Several *salen*-based complexes and their structure in assembled materials may result in interesting final properties and applications, like gas storage and CO_2 valorization. Other crucial application fields, considering current societal challenges, are the development of new systems for clean energy conversion and storage, new sensors for selective determination of vital ions, species and biological compounds and new eco-sustainable catalytic processes for the fabrication of important organic compounds.[10]

1.2. DACH in Chiral Discrimination, Molecular Recognition and Supramolecular Chemistry

The enantiomers of 1,2-DACH were recently exploited as guest model molecules in many cases with the goal of chiral discrimination and *ee* determination. Among the investigated hosts, binaphthyl-linked diporphyrin tweezers and an oxo-vanadium(V) aminotriphenolate complex can lead to chiral separations based on stereoisomer differentiation.[11] (1R,2R)-DACH was interestingly exploited in the study of the substitution of two pyridine ligands (py) in the complexes Δ- or Λ-$[Ru(bpy)_2(py)_2]^{2+}$ and Δ- or Λ-$[Ru(phen)_2(py)_2]^{2+}$ with retention of the absolute configuration. This allowed to successfully synthetize and characterize all the possible isomers of some ruthenium dinuclear complexes, with Δ- or Λ-$[Ru(bpy)_2(py)_2]^{2+}$ and Δ- or Λ-$[Ru(phen)_2(py)_2]^{2+}$ serving as enantiomerically-pure chiral building blocks in the preparation of complexes with defined stereochemistry.[12]

At the interface between the "host-guest" chemistry and molecular sensing, the synthetized library of DACH-based bis-binaphthyl macrocycles (S)-/(R)-5, both cyclic and acyclic ones, with the (S)-isomer reported in Figure 3 being an enantioselective fluorescent sensor for the recognition of chiral acids, such as the α-hydroxycarboxylic acid.[13]

DACH can play a key role also in helical supramolecular assemblies, for instance those made up of chiral polytriazoles carrying a TPE (teraphenylethene) backbone and a chiral L-phenylalanine (Phe) pendant. These aggregates showed excellent aggregation-induced emission, CD and CPL properties when the acid form of Phe was further added with chiral (1S,2S)-DACH. Dramatic changes in the intramolecular and intermolecular interactions indeed occur, affecting both chiral self-assembly and final optical properties, paving the way to

Fabio Piccinelli is Associate Professor of Inorganic Chemistry at the University of Verona. He received his MSc and PhD from the University of Bologna (2002 and 2006). He was a postdoctoral researcher at the Universities of Sheffield (2006), Bologna (2007) and Verona (2008). His research interests relate to the design, synthesis, structural and spectroscopic characterization of luminescent lanthanide-based complexes.

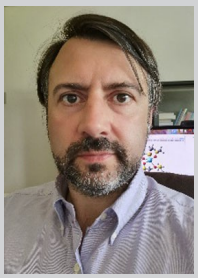

Andrea Melchior is Associate Professor of Chemical Foundations of Technologies at the University of Udine. He received his MSc in Chemistry at the University of Trieste (2000) and PhD in Chemical Technologies at the University of Udine (2004). He was subsequently a postdoctoral researcher at CEA Grenoble (2005), Udine (2006–2009) and the University of Seville (2009–2011). His research interests relate to the definition of the thermodynamic properties and structure of metal ions and complexes in solution and at the interfaces by means of computational and experimental approaches.

Lorenzo Di Bari is Professor of Organic Chemistry at the University of Pisa, where he has been head of the Department of Chemistry and Industrial Chemistry since 2018. He received his MSc and PhD from the University of Pisa and the Scuola Normale Superiore. His interests cover experimental methods for molecular and supramolecular stereochemistry.

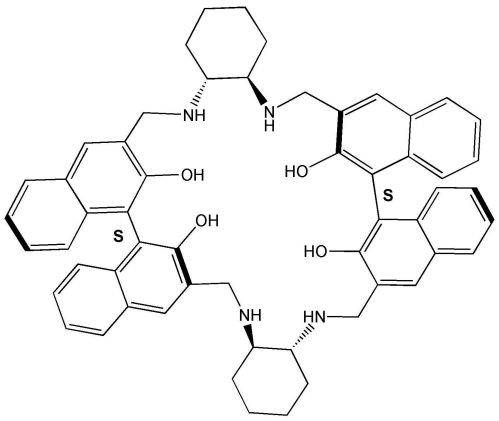

Figure 3. Molecular structure of DACH-based (S) isomer of the bis-binaphthyl macrocycles discussed in Ref. [13].

new opportunities in the development of optoelectronic devices.[14]

Remaining in the field of materials for advanced optical applications, it is worth to be mentioned a molecule bearing the perylene diimide (PDI) moiety linked to the DACH chiral scaffold. Interestingly, it exhibits a CPL emission ($g_{Em} \approx 10^{-3}$; *vide infra* for the definition of g_{Em}) and a two-photon absorption (TPA) process.[15] This simple structure (Figure 4) represents one of the few examples of purely organic compounds characterized by high values of molar absorptivity and luminescence quantum yield and combining both TPA and CPL responses.

Self-assembly forming well-defined rotationally displaced dimers affects the spectroscopic properties of the aggregate, giving rise to a shift of the emission into the near-infrared (NIR, 650–750 nm) spectral region.

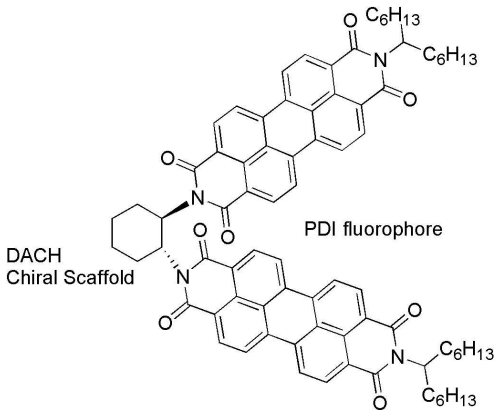

Figure 4. Chemical structure of the molecule discussed in Ref. [15].

1.3. DACH in Biochemistry, Pharmaceutics and Metal Ion Extraction

Very recently K. Kato et al.[16] reported the synthesis of four potential drugs, investigating their DNA-cleavage activity in the presence of $FeSO_4$ and sodium ascorbate. The development of DNA-cleavage reagents which recognize specific sequences will permit indeed oncological therapies with reduced side effects. These novel compounds – (1R,1′R,2R,2′R)-N1,N1′-(meta/para-phenylenebis(methylene))bis(N2,N2-bis (pyridin-2-ylmethyl) DACH) and their enantiomers – are optically active ligands and can coordinate two iron centers. The combined effect of the DACH stereochemistry and para-/meta-substitution of the xylene unit influence the efficiency and specificity of DNA cleavage, with p-R-BDC resulting the best derivative (compound **V**, Figure 5), also showing the ability to recognize a palindrome sequence.

Remaining in the pharmaceutical field, in 2015 G. Natile et al. reviewed the effect of chirality in platinum-based drugs. In the wake of the clinical success of cisplatin, other compounds were approved by authorities worldwide, including oxaliplatin (compound **VI**, Figure 5), FDA-approved in 2002. Such a drug contains the (R,R)-enantiomer of DACH as a ligand. Oxaliplatin gained increasing attention in the scientific community not only for its intrinsic chirality but also for its lack of cross-resistance with cisplatin. The bulkier and more hydrophobic nature of the R,R-DACH chelating ligand (compared to two ammonia molecules in cisplatin) accounts for a different interaction with DNA polymerases, mismatch repair proteins and damage recognition proteins. In other words, the DNA adducts of the R,R-DACH (*trans* form) complex are different, of course, from those of the S,S-DACH (*trans* form) and R,S-DACH (cis form; *meso*) platinum derivatives but also differ from those of cisplatin in cisplatin-resistant tumors. Therefore, from the molecular point of view, different underlying mechanisms of recognition and processing of platinum-DNA adducts led to the FDA-approval of oxaliplatin.[17]

Interestingly, the Janice R. Aldrich-Wright's research group reported the higher biological activity of a Pt(II)-based

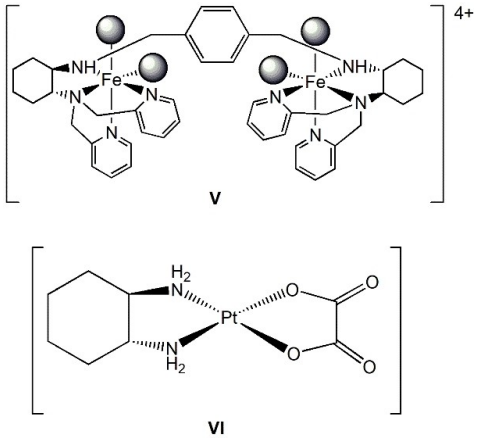

Figure 5. Chemical structure of p-R-BDC derivative (compound **V**) and oxaliplatin (compound **VI**). Grey spheres represent solvent molecules.

complex containing the (S,S)-enantiomer of DACH. The authors replaced the chloride ligands in the complex [$PtCl_2$(phen)], wherein phen is short form of 1,10-phenanthroline, with the ancillary chelating ligands R,R- and S,S-DACH. In all the 13 tested human cancer cell lines, the cationic complex $[Pt(S,S\text{-DACH})(phen)]^{2+}$ proved more cytotoxic than the R,R-enantiomer as well as cisplatin, recording IC_{50} values < 1 μM (72 h or 96 h treatment).[18]

In the field of lanthanide and actinides ion extraction, the well-known hydrophilic complexing agent CDTA (trans-1,2-DACH-N,N,N′,N′-tetraacetic acid), used as a "masking agent", is able to suppress the interference caused by the co-extraction of Zr(IV) and Pd(II), even in highly acidic conditions, when extracting lanthanides (Ln(III)) and minor actinides (An(III)), such as americium and curium.[19,20]

1.4. Lanthanide Ions and their Complexes

Due to the potential applications in several fields, lanthanide-based complexes have been broadly investigated, and their kinetic and thermodynamic of formation, as well as their structure have been analyzed. In this context, helpful studies have been performed by the research group of J. Lisowski.[21] By using several physical and theoretical methods, such as NMR, X-ray diffraction and DFT calculations, these authors investigated several DACH-based lanthanide complexes of macrocycles containing pyridine[21–24] or phenolic rings.[25] They were able to determine the structure of each species (with the corresponding kinetic or thermodynamic stability) in solution and of supramolecular assemblies whose formation is promoted by ion-pair interactions.

With respect to lanthanide ions, their properties, and the advantages of using their complexes for different applications, the three following sections touch upon the luminescence as well as the CPL (Circularly Polarized Luminescence) deriving from *f-f* transitions, followed by the thermodynamics of Ln(III)-based complexes.

1.4.1. Luminescence Originating from f-f *Transitions of Lanthanide Ions*

Trivalent lanthanide (Ln) ions having electronic configuration from $4f^1$[Ce(III)] to $4f^{13}$ [Yb(III)] are endowed of exceptional spectroscopic properties in the visible and near IR regions. This behavior makes them both extremely interesting in fundamental science, and outstanding light-emitting centers, useful in a wealth of applications, ranging from optical probes for bioimaging, to phosphors for light emitting diode (LED) lighting. Almost all the optical features of these ions are due to 4f-4f transitions, connecting $^{2S+1}L_J$ multiplets of the free Ln ions that are only weakly perturbed by the surrounding ligand field. The mechanisms responsible for these optical features belong to two different types: electric dipole (ED) and magnetic dipole (MD) transitions. For a detailed discussion of the ED and MD 4f-4f intra-configurational transitions the reader is referred to the very useful review by Peacock.[26] Other reviews are also recommended.[27,28]

It is important to remind that the ED transition operator has odd parity and therefore 4f-4f intra-configurational transitions, connecting levels formed by orbitals having the same parity, are at first order forbidden by the parity (Laporte) selection rule. For this reason, at first order only MD transitions are allowed, the MD transition operator possessing even parity. However, ED transitions can be experimentally observed due to the mixing of the $4f^n$ configurations with opposite parity $4f^n$-$5d^1$ ones due to odd parity operators (e.g. the ligand field). In this case the f-f transitions are allowed by the so-called forced ED mechanism, described by the Judd-Ofelt theory dating back to 1962.

The forced ED, and MD transitions for $^{2S+1}L_J$ multiplets are characterized by the following selection rules Forced ED transitions: $|\Delta J| \leq 6$ MD transitions: $\Delta J = 0, \pm 1$ (not $0 \leftrightarrow 0$). Weaker selection rules are operative on L and S.[26]

We also remind that MD transitions are in general at least an order of magnitude weaker than forced ED transitions. The forced ED absorption transition rates significantly depend on the local and electronic structure surrounding the Ln(III) ion, whilst the MD transition probability depend only on the refractive index of the host material. A complete list of all possible MD transitions for all Ln(III) ions is reported in Ref. [29], together with calculated emission rates and absorption oscillator strengths.

The quantum efficiency of the emission originating from a given excited level of a Ln(III) ion is affected by the presence of non-radiative decay channels that compete with the radiative emission of photons. The main non-radiative processes that depopulate an excited state are multiphonon relaxation (MPR) and energy transfer (ET).

MPR depends on the interaction between electronic states and vibrational modes present around the emitting center and can be strongly enhanced by increasing temperature.[30] In the case of Ln(III) ions, the MPR rate at a given temperature depends on the energy gap separating the emitting level from the one immediately below, and on the vibrational energies present in the material.[30,31] As a rule of thumb, MPR can be competitive with radiative decay when the number of vibrational quanta required to bridge this gap is lower than 5–6.[32] A comprehensive review of this topic in the case of molecular complexes can be found in Ref. [33].

On the other hand, ET depends on the non-radiative interaction between the electronic clouds of two optical centers (identical or not) located on different sites in the material. This interaction can transfer the excitation from one center (donor) to another (acceptor), thus leading to the depopulation of the excited levels of the donor (and the population of the acceptor's ones). The probability of this process depends on the distance between the donor and the acceptor, and the overlap between their respective emission and absorption spectra. In molecular complexes, ET can be important for the excitation of a metallic ion through transfer from an organic donor (antenna). The interested reader is referred to reviews on this subject.[34,35]

1.4.2. Circularly Polarized Luminescence (CPL) from f-f *Transitions of Lanthanide Ions*

Ln(III)-based circularly polarized luminescence (CPL) has some unique features, which we shall briefly review.

The first condition to achieve CPL is that both the electric (μ_{ij}) and magnetic ($\boldsymbol{m}_{ij}$) dipole vectors of the electronic transition ($i \rightarrow j$) under observation must be: a) non-zero; b) non orthogonal to one another.

This is because the quantity which governs optical activity, including CPL, is the rotational strength R_{ij}, that is the dot product between the two transition dipoles [Eq. (1)]

$$R_{ij} = \mu_{ij} \cdot \boldsymbol{m}_{ij} \tag{1}$$

R_{ij} is proportional to the difference of intensity of left (I^L) vs. right (I^R) CP-light [Eq. (2)]

$$R_{ij} \propto I^L - I^R = \Delta I \tag{2}$$

We can consider the two conditions a) and b) above separately.

Condition a) non zero electric and magnetic dipole moments for the same electronic transition. Purely intra-configurational *f-f* transitions of a Ln(III) ion should be Laporte forbidden and display vanishing electric dipole moment to first order. This is responsible for the absorption spectra of lanthanide ions and for the need of the antenna effect to promote their luminescence. Coupling with vibrational states introduces a perturbation, which may overcome this limitation, depending on the angular quantum numbers (L, S, J) of the two electronic states (i and j). For example, the well known $D_0 \rightarrow F_2$ transition of Eu(III) has $\Delta J = 2$ and becomes electric-dipole allowed, but magnetic dipole forbidden. This transition gives rise to the bright red-orange emission line at 615 nm of many Eu(III) compounds. Just at the opposite, the $D_0 \rightarrow F_1$, which falls around 595 nm, is electric dipole forbidden, but magnetic dipole allowed.

If the coupling with the environment allows to relax both prohibitions to some extent, and the two mentioned transitions may acquire some of the lacking character (*magnetic* moment for $D_0 \rightarrow F_2$ or *electric* character for $D_0 \rightarrow F_1$) and both become CPL-active, possibly to a comparable extent.

Rotational strength, however, is not the most relevant feature one needs to consider. In fact, rather than ΔI, it is worth considering the *fraction* of photons of one handedness with respect to the *total* number of emitted photons. This is expressed by the so-called emission dissymmetry factor g_{Em} [Eq. (3)]:

$$g_{Em} = \frac{2\left(I^L - I^R\right)}{I^L + I^R} \tag{3}$$

From the point of view of g_{Em}, the two transitions of Eu(III) can be very different, because the electric-dipole allowed $D_0 \rightarrow F_2$ can be much more emissive than the $D_0 \rightarrow F_1$, which remains forbidden to a higher order. Thus, we may put forward that $D_0 \rightarrow F_2$ can be expected to have smaller g_{Em} than $D_0 \rightarrow F_1$.

In a seminal paper of 1980, based on perturbation theory, Richardson defined optical activity selection rules for Ln(III) ions which can be found in detail Ref. [36]. He classified Ln(III) transitions as E*I*, E*II*, E*III*, for decreasing electric-dipole character, R*I*, R*II*, R*III*, for decreasing rotational strength and D*I*, D*II*, D*III* for decreasing dissymmetry factor.

Table 1 summarizes some of the transitions, which have been investigated for Ln(III)-centered optical activity.

Returning back to the conditions listed above, let us focus on the requirement b) non orthogonal electric and magnetic dipole moments. This is eminently a condition allied to the geometry of the Ln(III) environment.

It may be worth recalling that any improper symmetry element (inversion, mirror planes, rototranslation axes) are incompatible with chirality and can be discarded. There remain only proper elements (rotation axes) as present in C_n or D_n point groups. Let us assume that the Ln(III) complex has a C_n symmetry axis $(n \geq 2)$. This immediately implies that, along that axis the two moments must be collinear and that, apart from the sign (which depends on the *absolute geometry*) their dot product reduces to [Eq. (4)]:

$$R_{ij} = \mu_{ij} \cdot \boldsymbol{m}_{ij} = \pm|\mu_{ij}| \cdot |m_{ij}| \tag{4}$$

(NB the angle between μ_{ij} and $\boldsymbol{m}_{ij}$ is either 0° or 180° and its cosine is ± 1).

This condition allows us to reduce the expression for g_{Em} for a specific transition $(i \rightarrow j)$ to the particularly simple form [Eq. (5)]:

$$g_{Em}(i \rightarrow j) = \pm \frac{4|\mu_{ij}| \cdot |m_{ji}|}{|\mu_{ij}|^2 + |m_{ji}|^2} \tag{5}$$

Which reaches its maximum (absolute value) $g_{Em}(i \rightarrow j) = \pm 2$ when [Eq. (6)]:

$$|\mu_{ij}| = |m_{ji}| \tag{6}$$

For complexes of lower symmetry, or for transitions which are not aligned to a C_n axis, the two dipoles are no longer necessarily collinear, and in general the cosine may not be

Table 1. Richardson's classification of Ln(III)-centered transitions.[36]

Ln	Transition	λ	Classification
Eu	$^5D_0 \rightarrow {}^7F_1$	590 nm	*EIV RIII DI*
	$^5D_0 \rightarrow {}^7F_2$	613 nm	*EII RIII DIII*
	$^5D_0 \rightarrow {}^7F_3$	650 nm	*EIV RIV DII*
Sm	$^4G_{5/2} \rightarrow {}^6H_{5/2}$	565 nm	*EII RII DI*
	$^4G_{5/2} \rightarrow {}^6H_{7/2}$	598 nm	*EII RII DI*
	$^4G_{5/2} \rightarrow {}^6H_{9/2}$	640 nm	*EII RII DIII*
Yb	$^2F_{5/2} \rightarrow {}^2F_{7/2}$	980 nm	*EI RI DII*
Tm	$^3H_5 \rightarrow {}^3H_6$	1210 nm	*EI RI DII*
Tb	$^5D_4 \rightarrow {}^7F_6$	490 nm	*EII RIII DIII*
	$^5D_4 \rightarrow {}^7F_5$	545 nm	*EII RII DII*
	$^5D_4 \rightarrow {}^7F_4$	585 nm	*EII RII DII*
	$^5D_4 \rightarrow {}^7F_3$	622 nm	*EII RII DII*

omitted. Nonetheless, the largest $g_{Em}(i \rightarrow j)$ is met when $|\mu_{ij}| = |m_{ji}|$, although it is no longer ± 2.[37]

There is a further aspect, which is peculiar to Ln(III) CPL, which is easily overlooked, although it may play a most relevant role.

Except for a very few cases, Ln(III) centered term-to-term transitions are manifolds due to M_J components. This means that they consist in a set of lines, which are separated from one another by crystal field splittings (CFS). Typical CFS amounts to one or a few hundreds of wavenumbers. Each line will have its own transition probability (total strength), but, more importantly, its own R_{ij}, including the sign. The emission spectrum will consist of a set of (very) closely spaced lines. Sometimes, at room temperature the natural linewidth itself may be comparable or even exceed the separation between the lines. Furthermore, very commonly, in order to collect more light during the measurement, one opens up the instrument slit, at the expenses of resolution. In the total luminescence (TL) spectrum, this has the consequence of introducing a broadening of the lines, which may appear smeared out, with some loss of information. Often, this can be acceptable, due to the unquestionable gain in signal-to-noise. In CPL, however, any loss in resolution should be carefully avoided, because of the possibility that neighbor lines have oppositely signed R_{ij}. In such an occurrence, if they are at least partly overlapped, because of natural or instrumental linewidth together with limited spacing, they would mutually cancel out, at least to some extent. This effect is highly detrimental, and the emission monochromator slits must be carefully adjusted, for each specific case.

A further reason for observing a multitude of lines in Ln(III) emission spectra arises from the fact that when the CFS terms are small compared to kT (at room temperature, $kT \cong 200\ cm^{-1}$) so called hot-bands will also be seen, arising from the Boltzmann population of substates above the ground level.

Ln(III) TL luminescence spectra have been indicated as spectroscopic barcodes, thanks to their rich manifolds of lines, with very well defined wavenumbers and relative intensities which are absolutely typical of the compound under investigation. This is all the more true for CPL, which takes advantage of the sign information.

1.4.3. Speciation of Ln-Based Complexes

In vitro or *in vivo* applications of Ln(III) complexes for sensing or imaging purposes require the ligand protonation and complex formation equilibria to be well defined in order to know the emitting species present at given conditions (e.g. pH). The ligand containing the *antenna* should have several characteristics: *i*) to form a thermodynamically stable complex in solution, in order to avoid the release of the metal ion, especially in complex matrixes where competing species (e.g. Ca^{2+}, Zn^{2+}, $Cu,^{2+}$…) can be present; *ii*) to be sufficiently soluble in the free and complexed form; iii) to leave some coordination sites accessible to incoming analytes in order to exert the sensing function. Ligands designed to obtain a high thermodynamic stability with Ln(III) ions contain hard donor atoms, as these metal ions behave as hard acids with a strong affinity for hard bases like O-donors (neutral or negatively charged) or N-donors with which they form essentially bonds of a predominant ionic nature.[38–40] Besides the intrinsic metal-donor affinity based on the HSAB theory,[41] the factors which influence the thermodynamic stability of the formed species include charge neutralization, desolvation/solvation of the reagents and products, chelate and macrocyclic effects.[42] Protonation and complex formation constants data can be obtained experimentally by analyzing potentiometric or combined potentiometric/spectrophotometric titration data in aqueous solutions.[43] Also, isothermal titration calorimetry (ITC) is a useful tool to obtain the reaction enthalpies and, when the ΔG° is also known, to calculate the associated entropy changes.[44,45] Besides the thermodynamic parameters, the analysis of NMR and UV-Vis titration data also allow to obtain structural information, namely the sequence of protonation sites and the groups with which the metal ion is interacting at different pH.[39,46]

Metal speciation can be determined also in non-aqueous solvents by employing spectroscopic,[47] calorimetric[38,48] and in some cases[49] potentiometric methods. In non-aqueous media, attention should be paid to the composition of the solution, particularly to the water content,[50,51] as H_2O molecules can compete with weakly coordinating solvents for the metal ion and to the possible coordination of the counterions.[38]

The knowledge of the equilibria in solution allows to define the starting system when sensing experiments are carried out. In the latter applications, the formation of ternary ML-analyte species is monitored at fixed conditions (most often physiological pH and ionic medium) and conditional formation constants are determined. A variety of methods have been employed, such as fluorimetry, spectrophotometry, NMR, and calorimetric titrations.[52–54] In some cases,[53] the combination of different techniques and computational methods is necessary to distinguish between different speciation models (*vide infra*).

2. Luminescent Chiral Lanthanide-Based Complexes Containing *trans*-1,2-Diaminocyclohexane (DACH)

In the following sections, we reviewed the spectroscopic properties and the potential applications of luminescent, chiral lanthanide complexes containing DACH fragment, which have been discussed so far in the literature.

2.1. Complexes Containing:

a) N,N,N′,N′-tetrakis(2-pyridylmethyl)-*trans*-1,2-diaminocyclohexane (tpdac)

b) 6,6′-[(cyclohexane-1,2-diylbis{(carboxymethyl)azanediyl}) bis(methylene)]dipicolinic acid (H_4cddadpa)

c) 2-hydroxyisophthalamide (IAM) antenna as Chromophore (cyLI-IAM)

The research group of G. Ung designed several luminescent complexes of Sm(III), Eu(III), Tb(III) and Dy(III) of the chiral tpdac ligand[55] (Figure 6) exhibiting CP emission with strong dissymmetry factors, when dissolved in acetonitrile.

In particular, upon UV excitation around 280 nm, while as expected for Sm(III), the related enantiopure complexes show the highest g_{Em} value (|0.12|) in correspondence of $^4G_{5/2}\rightarrow{}^6H_{5/2}$ transition around 563 nm. In the case of Eu complex, surprisingly, stronger CPL signals (~ |0.08|) were observed from the $^5D_0\rightarrow{}^7F_3$ and $^5D_0\rightarrow{}^7F_4$ at 650 and 701 nm, respectively. The latter transitions normally do not exhibit stronger CPL signals than the typically studied $^5D_0\rightarrow{}^7F_1$ and $^5D_0\rightarrow{}^7F_2$ transitions. As for the Tb(III)-based complexes, more surprisingly, the weakly emissive $^5D_4\rightarrow{}^4F_2$ transition at 653 nm exhibits a very strong CPL signal with a g_{Em} of |0.22|, which is not consistent with the transition rules described by Richardson (Table 1).[36] The unusual CPL activity of the Eu(III) and Tb(III) complexes may be attributed to a peculiar ligand crystal field, associated to a single C_2-symmetrical species. If compared to similar chiral complexes containing 2, 2′-pyrrolidine and bipyridyl chromophore investigated by the same authors[56] and showing sizeable g_{Em} values, the presence of DACH backbone seems to confer the peculiar aforementioned chiroptical properties to the lanthanide complexes.

Compared to non-macrocyclic Gd(III) complexes approved as MRI contrast agents for clinical use, the anionic, water-soluble and highly stable complexes of Gd(III) and Eu(III) with the cddadpa ligand investigated by G. Tircsó et al.[57] show a superior kinetic inertness by 2–3 orders of magnitude and comparable to those of macrocyclic complexes (Figure 7). This unusual feature is due to the rigidifying effect of the diaminocylohexane unit in the ligand skeleton (half-life of dissociation for physiological conditions is 6 orders of magnitude higher for $[Gd(cddadpa)]^-$ ($t_{1/2}=1.49\cdot10^5$ h) than for $[Gd(octapa)]^-$; (octapa contains the flexible ethane bridge instead of cyclohexane unit). Despite its favorable kinetic and thermodynamic properties, the luminescence spectroscopy of the $[Eu(cddadpa)]^-$ complex has not been investigated yet.

The unexpected presence in aqueous solution of a single species with C_1 symmetry could have an important impact on the chiroptical properties of this molecule and in this direction, a spectroscopic investigation on a series of luminescent Ln(III) complexes would be interesting to be carried out.

The cyLI-IAM ligand (Figure 8) forms a 2:1 ligand/Tb(III) complex displaying both large luminescence quantum yield (ϕ) values (around 60%) and strong CPL activity (g_{Em} = |0.2|) in correspondence to the $^5D_4\rightarrow{}^7F_5$ transition, when dissolved in aqueous solution at physiological pH, as reported by the research group of K. N. Raymond.[58]

The crucial role of the rigid DACH backbone is again evident. The increased rigidity of the ligand, when compared with the similar molecule possessing the diphenylethylenediamine (dpenLI) chiral unit, seems responsible for the higher values of the emission quantum yield and g_{Em}. Varying the chiral diamine was found also to impact solvent access to the Tb(III) center and the speciation in solution. Only one species without solvent molecules in the inner coordination sphere of the metal ion is observed in the case of $(CyLI\text{-}IAM)_2Tb$ complex. A similar behavior was found when a Tb(III) complexes of an octadentate chiral DACH-based ligand containing four IAM *antennae* was employed.[59] In this case, the value of g_{Em} around 545 nm was lower (|0.08|).

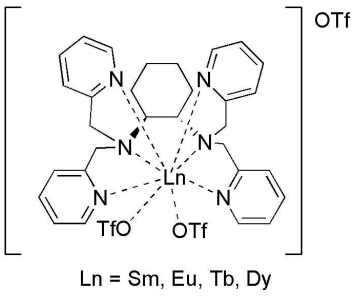

Figure 6. Ln(III) complexes of the ligand (R,R) or (S,S)-tpdac discussed in the paper by G. Ung and co-authors.[55]

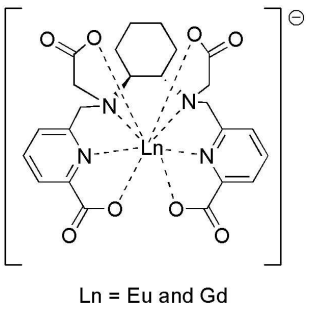

Figure 7. Ln(III) complexes of the ligand (R,R) or (S,S)-cddadpa discussed in the paper by G. Tircsó and co-authors.[57]

2.2. Ligands Containing Nitrogen-Based Heteroaromatic Chromophores such as Pyridine, Quinoline and Isoquinoline and their Water Soluble Eu(III) and Tb(III) Complexes

2.2.1. Thermodynamic and Structural Characterization

Ln(III) complexes of the achiral ligand H_2bped (Figure 9) are expected highly stable in aqueous solution, as demonstrated by the value of the stability constant in the case of its Gd(III) counterpart ($\log\beta=12.37$).[60]

The potential use in the biosensing field of bped-like lanthanide complexes has been developed by the research

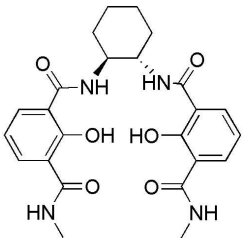

Figure 8. CyLI-IAM as ligand of Tb(III).[58]

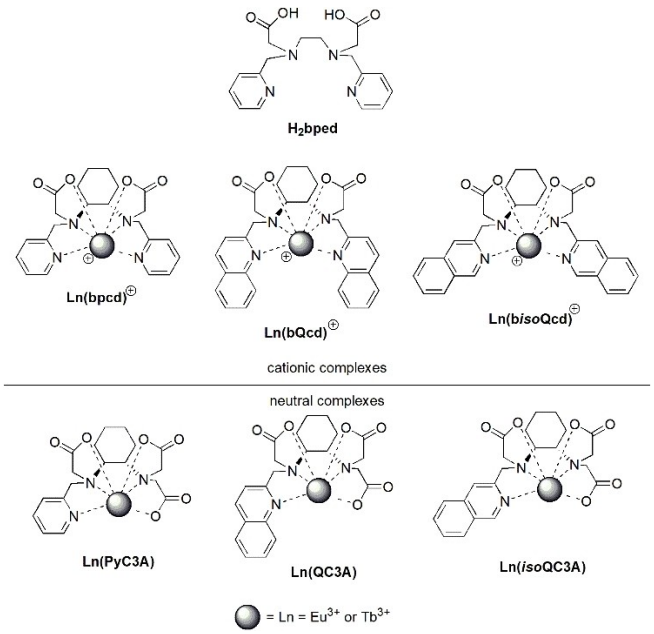

Figure 9. Chemical structure of H_2bped ligand and of the Eu(III) and Tb(III) complexes discussed in section 2.4. $bpcd^{2-}$ = N,N′-bis(2-pyridylmethyl)-trans-1,2-diaminocyclohexaneN,N′ diacetate; $bQcd^{2-}$ = N,N′-bis(2-quinolinmethyl)-trans-1,2-diaminocyclohexane N,N′-diacetate; $bisoQcd^{2-}$ = N,N′-bis(2-isoquinolinmethyl)-trans-1,2-diaminocyclohexane N,N′-diacetate; $PyC3A^{3-}$ = N-picolyl-N,N′,N′-trans-1,2-cyclohexylenediaminetriacetate; $QC3A^{3-}$ = N-quinolyl-N,N′,N′- trans-1,2-cyclohexylenediaminetriacetate; $isoQC3A^{3-}$ = N-isoquinolyl N,N′,N′-trans-1,2-cyclohexylenediaminetriacetate.

groups of F. Piccinelli, L. Di Bari and A. Melchior. The characterization of solution equilibria provided the protonation constants (reported as logK_n in Table 2) which were included in the model for the determination of complex formation constants (logβ).

The "chiral version" (H_2bpcd) of this ligand, containing the DACH moiety, was prepared in 2017 and has been shown[61] to form highly stable complexes with Eu(III) and Tb(III) ions at room temperature with logβ values for the Ln(bpcd) species in the 11.2–11.4 range (Table 3 and Figure 9). In this case, the increased rigidity of this ligand with respect to H_2bped causes a slight decrease of stability. This is somewhat unexpected on the basis of the preorganization effect[42] as, for example, found when comparing the stability of complexes formed by Eu(III) with EDTA and CDTA.[62] However, this difference could be assigned to *i)* the fact that bpcd and bped have only two carboxylate groups and therefore the extra stability due to preorganization is expected to be lower; *ii)* the pyridine groups present less degrees of freedom than acetates.

Table 3. Formation constants (logβ) of Eu(III) and Tb(III) complexes, reported in Figure 9, at T = 298.15 K and μ = 0.1 M NaCl. Charges are omitted for clarity.

Reaction	bpcd[a]	bQcd[b]	PyC3A[b]	QC3A[b]
L + Eu ⇆ EuL	11.2	9.97	15.68	12.6
L + Eu ⇆ EuL(OH) + H	2.2	–	–	–
L + Tb ⇆ TbL	11.35	9.8	15.70	12.1
L + Tb ⇆ TbL(OH) + H	2.1	–	–	–

[a] Ref. [61]. [b] Ref. [63].

Table 4. Formation constants (logβ) of Eu(III) complexes reported in Figure 9, at T = 298.15 K and μ = 0.1 M NaCl. Charges omitted for clarity.

Reaction	*biso*Qcd[a]	*iso*QC3A[b]
L + Eu ⇆ EuL	10.53(4)	14.6(1)

[a] Ref. [53]. [b] Ref. [52].

C.C. McLauchlan et al. showed that, although the [Ln(bpcd)] PF_6 complexes are C_2-symmetric single species in solution, the La-based derivative crystallizes as binuclear complex with $[La_2(bpcd)_2(H_2O)_2]^{2+}$ formula.[64]

The change of the heteroaromatic chromophore was also considered and quinoline and *iso*quinoline rings have been incorporated in the ligand structure. Taken together, six ligands and the related Eu(III) and Tb(III) complexes have been prepared (Figure 9). When an aromatic ring is substituted by an acetate fragment, neutral complexes are obtained [Ln(PyC3A); Ln(QC3A) and Ln(*iso*QC3A)]. These complexes are more stable than the cationic counterpart [i.e. Ln(PyC3A) *vs.* Ln(bpcd)$^+$; Tables 3 and 4]. This is likely due to the stronger interaction of the acetate oxygen with respect to the heteroaromatic nitrogen and the entropically favorable charge neutralization taking place during the complexation of Ln(PyC3A), Ln(QC3A) and Ln(*iso*QC3A).

On the other hand, the Eu(III) and Tb(III) complexes containing quinoline rings are less stable (log$\beta \sim 10$). As this family of ligands presents six donating atoms not capable to saturate the coordination sphere of the metal ion, solvent molecules can also bind the cation. DFT calculations performed on all the Y(III) analogues, as its complexes present similar structural features to Eu(III) but have no unpaired electrons, thus improving the speed of calculation,[61] considering solvent explicitly, revealed the presence of two water molecules directly bound to Y(III) (Figure 10). This result was confirmed also by calculations where up to 5 water molecules were added in the proximity of the metal ion which produced all final

Table 2. Protonation constants (logK_n, $K_n = [LH_n]/([H]\cdot[LH_{n-1}])$) of the ligands reported in Figure 9, at T = 298.15 K and μ = 0.1 M NaCl.

	bpcd[a]	bQcd[b]	*biso*Qcd[c]	PyC3A[b]	QC3A[b]	*iso*QC3A[d]
logK_1	9.72	9.87	9.27	10.26	10.53	9.43
logK_2	5.87	5.85	5.86	6.33	6.29	7.37
logK_3	2.94	3.46	3.43	3.67	3.60	3.32
logK_4	2.22	1.79	1.62	2.01	2.81	2.16

[a] Ref. [61]. [b] Ref. [63]. [c] Ref. [53]. [d] Ref. [52].

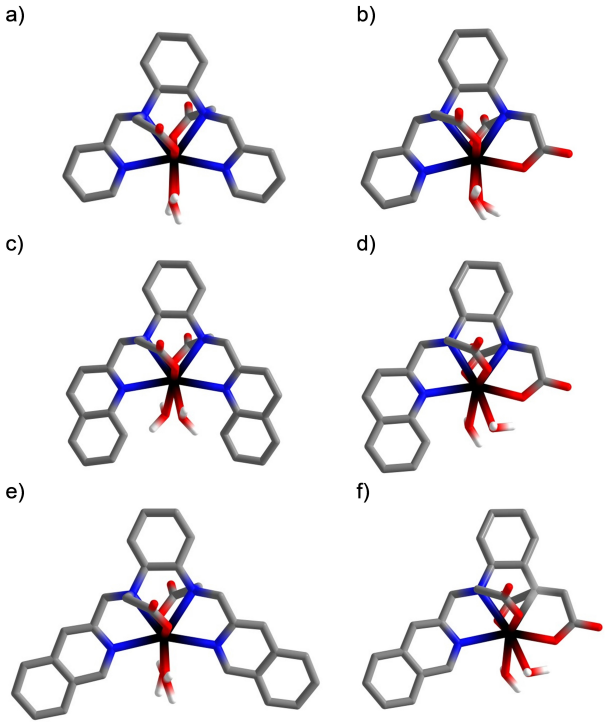

Figure 10. Minimum energy structures of (a) [Y(*trans*-O,O-bpcd)$(H_2O)_2]^+$; (b) Y(*trans*-O,O-PyC3A)$(H_2O)_2$; (c) [Y(*trans*-O,O-bQcd)$(H_2O)_2]^+$; (d) Y(*trans*-O,O-QC3A)$(H_2O)_2$; (e) [Y(*trans*-O,O-*iso*bQcd)$(H_2O)_2]^+$; (f) Y(*trans*-O,O-*iso*QC3A)$(H_2O)_2$. H atoms attached to carbons are omitted for clarity. Adapted from Refs. [52,63]. Copyright (2019) and (2021), with permission from the Royal Society of Chemistry.

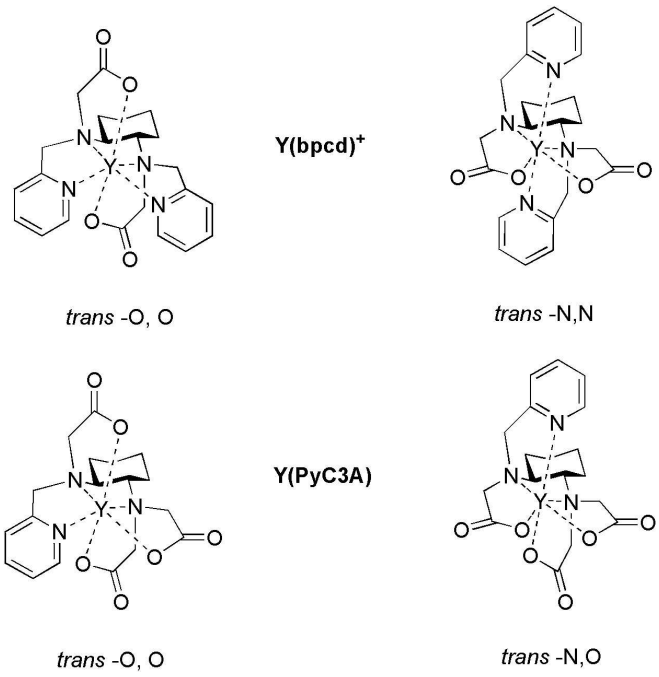

Figure 11. Possible stereoisomeric complexes found by DFT calculations. In the case of cationic complexes with $bpcd^{2-}$, $bQcd^{2-}$ and *iso*$bQcd^{2-}$ ligands, *trans*-O,O and *trans*-N,N species are observed. In the case of neutral complexes with $PyC3A^{3-}$, $QC3A^{3-}$ and *iso*$QC3A^{3-}$ ligands, *trans*-O,O and *trans*-N,O species are observed. Only the representative pyridine-based complexes are depicted in this figure. Water molecules bound to the metal ion are omitted for sake of clarity.

structures with only two waters directly bound and the others forming H-bonds in second sphere.[65]

In Figure 10, only one of the two possible stereoisomers of the complexes is reported (*trans*-O,O). Besides the *trans*-O,O isomers, the nearly equally stable *trans*-N,N and *trans*-N,O ones must be taken into consideration. In Figure 11, all possible isomers are depicted in the representative case of the pyridine-based complexes.

As can be evinced by the inspection of figure 10, the increased steric hindrance and the weaker interaction with the metal ion than in the case of pyridine are responsible for the drop of stability in the case of quinoline-based complexes. In line with this statement, we observed, on average, a longer Y(III)$-N_{heterocycle}$ bond distance when quinoline is considered ($\Delta Py \rightarrow Q \sim +0.11$ Å),[63] indicating the weaker interaction with the metal ion; this possibly contributes to the aforementioned drop of stability (on average ~1.4 and 3.4 log units for the di- and tri-acetate ligands). However, the impact on the solvation properties of the complex, also affecting the stability, due to the quinoline ring cannot be ruled out. As for the speciation in solution, in all cases only one species with a 1:1 ligand-to-metal stoichiometry was detected at physiological pH. In the case of Eu(III) and Tb(III) complexes with $bpcd^{2-}$,a small amount of an hydroxo complex is detected at pH > 8.[61]

2.2.2. Luminescence Spectroscopic Properties

As for potential application in the biomedical field, this family of Ln(III) complexes shows several interesting features. First, thanks to a ligand to metal energy transfer process (*antenna effect*) a tunable excitation wavelength in the UV region (around 270 nm or 320–330 nm, for pyridine and quinoline (or isoquinoline)-based complexes, respectively) is possible. The total charge of the complex, steric hindrance at the metal ion and lipophilicity can be also tuned: Ln(bpcd)$^+$, Ln(bQcd)$^+$ and Ln(*iso*bQcd)$^+$ are cationic whilst Ln(PyC3A), Ln(QC3A) and Ln(*iso*QC3A) are neutral. The steric hindrance at the metal ion is large in the case of Ln(bQcd)$^+$ and small in the case of Ln(PyC3A). Also, the compounds containing the quinoline (or isoquinoline) fragments are more hydrophobic than the corresponding pyridine-based ones. Finally, these complexes present metal coordination sites occupied by displaceable water molecules which can be easily replaced by target analytes giving rise to a distinct optical response. In fact, the displacement of water molecules by the target species often suppresses the MPR process giving rise to an increase in the luminescence emission quantum yield in such a way that the increase in the luminescence intensity could be linked to the concentration of the analyte in solution.

Total charge and steric hindrance are expected to have a strong impact on the stability of both the complexes and their adducts with target analytes to enable the opportunity of a selective probe-target interaction. On the other hand as for

in vitro experiments, lipophilicity and charge can strongly impact on the cell viability, cell uptake and membrane permeability.[66–71] In Figure 12a and 12b, the excitation and emission spectra for Eu(III) and Tb(III) complexes depicted in Figure 9, are respectively showed.

Depending on the nature of the chromophoric unit it is possible to tune the excitation wavelength of the molecule. Upon excitation of the ligand around 265 nm, in the case of pyridine-based complexes, an efficient emission stemming from Eu(III) and Tb(III) is detected (Figure 12a and b for the ligands $bpcd^{2-}$ and $PyC3A^{3-}$). On the other hand, the quinoline and isoquinoline-based ligands are capable to efficiently sensitize only the Eu(III) luminescence and no antenna effect is detected in the case of Tb(III) ion. The excitation wavelength is located around 318 nm in the case of $bQcd^{2-}$ and $QC3A^{3-}$; whilst it is red shifted (328 nm) in the case of isoquinoline-based complexes [Eu(isoQC3A) and $Eu(bisoQcd)^{+}$] (Figure 12a).

In all the studied cases, due to the chiral nature of the molecules prohibiting the inversion center as possible element of symmetry for the metal ion, the electric dipole $^5D_0 \rightarrow {}^7F_2$ band is dominant, and Eu(III) ion emits in a forced electric dipole regime. It is also noteworthy that the $^5D_0 \rightarrow {}^7F_0$ transition shows significant intensity for all the complexes, in agreement with the C_n, C_{nv} or C_s as possible Eu(III) point symmetries.[72] The number of coordinated water molecules have been also calculated spectroscopically, by means of the Horrock's equation[73,74] in which observed Eu(III) $^5D_0$ excited state lifetimes measured in water and D_2O are required. For all the Eu(III) complexes, the number of water molecules present in the inner coordination sphere (q) is in the 2.4–2.8 range. This result well agrees with what has been observed by DFT calculation if we consider that the hydration number (q) is also slightly sensitive to the presence of water molecules in the second coordination sphere.[74] Although the emission spectra and the single exponential profile of the decay curves of the Eu(III) excited state call for the presence of a single emitting species, the presence of two isomeric structures, suggested by DFT calculations, does not disagree with this spectroscopic evidence. In fact, these two species, possessing the same point symmetry (C_2), may show very similar Eu(III) luminescence emission spectra and the same transition energy of the $^5D_0 \rightarrow {}^7F_0$ band. In fact, the 0-0 transition energy is mainly determined by degree of covalency (nephelauxetic effect) of the bonds between the metal ion and the ligand.[75] This is, in turn, dependent on the coordination number of Eu(III), which is the same for the two isomers. As for the CPL spectroscopy, we measured the CPL spectra in CD_3OD for all the complexes described in Table 5, where the g_{Em} values are collected.

Clearly, sizeable values of g_{Em} are recorded for Tb(III) and Eu(III) complexes containing the $bpcd^{2-}$ ligand. In Figure 13a, the CPL spectrum of the two enantiomers of $[Tb(bpcd)^{+}]$ is reported both in CD_3OD and H_2O (Figure 13).

The spectrum in water retraces those measured in CD_3OD with a slightly lower g_{Em} value (0.07 at 546 nm). This suggests that, in principle, $[Tb(bpcd)]^{+}$ can be suitable as a CPL bioprobe for relevant analytes in aqueous media (see below), also in light of its higher emission intensity than the $[Eu(bpcd)]^{+}$; the latter compound being more affected by the MPR process. Finally, we demonstrated also that the CPL activity in $[Tb(bpcd)^{+}]$ and $[Eu(bpcd)^{+}]$ mostly falls in the static coupling limit.[61] This is expected, since the pyridine rings are weakly chromophoric, with transitions falling in the far-UV region.

Finally, the water soluble $Tb(bpcd)^{+}$ complex shows a good value of the CPL brightness, as defined by some of us.[76] This value (around 23 $M^{-1}cm^{-1}$) is below the median of Tb^{3+} complexes recently reported in the literature, but still significant in the context of water soluble complexes.[77]

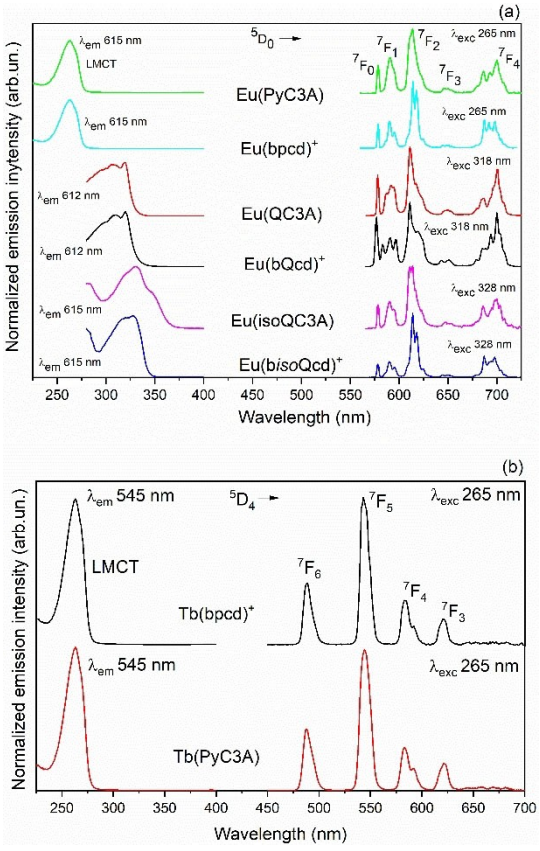

Figure 12. (a) Excitation and emission spectra of Eu(III) complexes depicted in Figure 9. (b) Excitation and emission spectra of Tb(III) complexes of the ligands $bpcd^{2-}$ and $PyC3A^{3-}$.

Table 5. g_{Em} values in deuterated methanol at different wavelengths, for the complexes depicted in Figure 9.

Compound	$\lvert g_{Em} \rvert$ (wavelength [nm])
$Eu(bpcd)^{+}$	0.2(598); 0.23(607); 0.14(625)
$Tb(bpcd)^{+}$	0.11(546); 0.16(585); 0.11(622)
Eu(PyC3A)	0.05(588); 0.043(609); 0.026(623)
Tb(PyC3A)	0.011(484); 0.019(539); 0.018(544); 0.017(551)
$Eu(bQcd)^{+}$	0.057(589); 0.097(596); 0.012(613)
Eu(QC3A)	0.016(591); 0.028(607); 0.004(619)
$Eu(bisoQcd)^{+}$	0.074(587); 0.033(596); 0.023(613); 0.014(621)
Eu(*iso*QC3A)	0.02(587); 0.01(610)

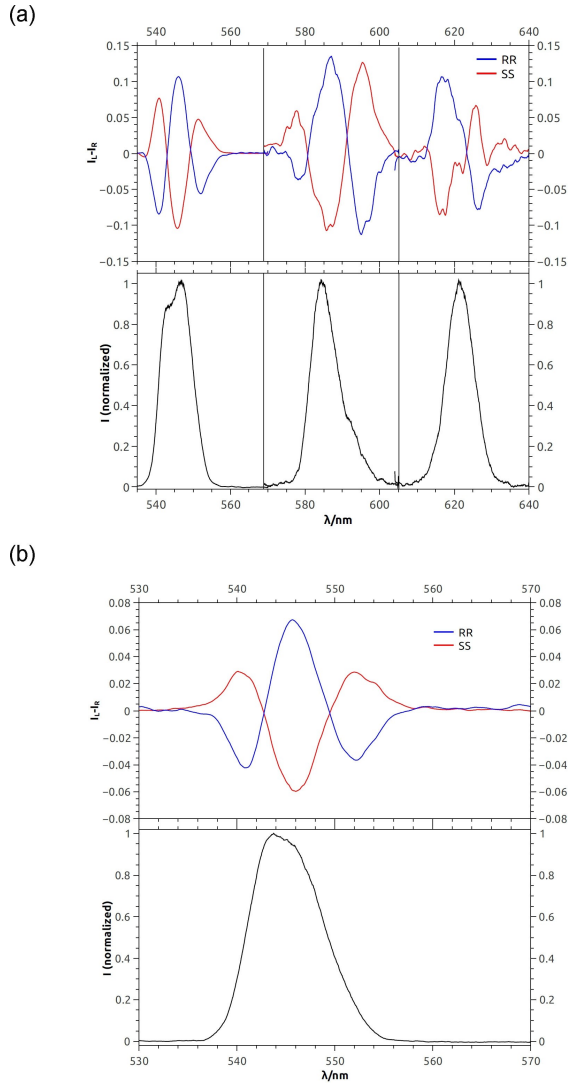

Figure 13. Normalized CPL spectra (top) and total emission (bottom) of the two enantiomers of Tb(bpcd)$^+$ in CD_3OD (a) and water (b). The curves in each panel are normalized on the maximum of the corresponding total emission band. Adapted with permission from Ref. [61]. Copyright (2017) American Chemical Society.

2.2.3. Sensing of Bioanalytes Present in a Typical Interstitial Extracellular Fluid

As far as the optical sensing of important bio-analytes is concerned, hydrogen carbonate, lactate, citrate, proteins, such as bovine and human serum albumins (BSA, HSA) have been widely investigated, since they are among the main species contained in an interstitial extracellular fluid. In addition, CPL spectroscopy can be conveniently used to reveal the interaction between a suitable luminescent Ln-probe and an analyte of interest.[78] CPL is extremely sensitive to the stereochemical surrounding of the metal center. Indeed, upon interaction with an analyte, it is possible that the total luminescence spectrum of the complex undergoes only minor or no variation, while the CPL spectra can display very significant variations in its shape and signature. It is also possible, to interact racemic complex (displaying no CPL) with chiral analytes and then observe the rise of a CPL signal induced by the analyte itself. In this way CPL acts as an on/off telltale signal.

2.2.3.1. Lactate

Both the enantiomers of [Tb(bpcd)$^+$] interact similarly and weakly with the L-lactate molecule, as the log value of the association constant was found to be 1.3-1.45, by means of luminescence titration and isothermal titration calorimetry.[79] L-lactate is capable to displace both the water molecules bound to the metal ion upon binding with carboxylic and hydroxylic groups (Figure 14a). As expected, this is responsible for an increase of both the Tb(III) emission intensity and $^5D_4$ excited state lifetime.

Despite their similar stability, the adduct between L-lactate and the (R,R) enantiomer of Tb(bpcd)$^+$ [(R,R)-L isomer] is less CPL active than the (S,S)-L adduct. Because of this peculiarity, the racemic mixture of Tb(bpcd)$^+$ can give rise to a CPL signal, when L-lactate is present in solution, as the negative signal of the (S,S)-L adduct is not completely counterbalanced by the positive one belonging to the (R,R)-L adduct. This has been clearly demonstrated also in a commercially available solution for medical use, containing several electrolytes, namely Ringer's lactate (Figure 14b). Although this result paves the way to the development of an analytical assay based on Tb luminescence in the visible window, the moderate stability of the adduct with L-lactate hampers the possibility to detect this molecule in more complex conditions close to real biological fluids, where other competitive anions (e.g. citrate, proteins, phosphate, bicarbonate…) are present.

2.2.3.2. Hydrogen Carbonate (HCO_3^-)

Although Eu(bQcd)$^+$, Eu(PyC3A), Tb(PyC3A) and Eu(QC3A) show an enhancement of their luminescence emission intensity upon addition of hydrogen carbonate in aqueous solution, we noticed an unprecedented affinity for HCO_3^- in the case of the Eu(bpcd)$^+$, Tb(bpcd)$^+$ complexes. In these cases, logK values

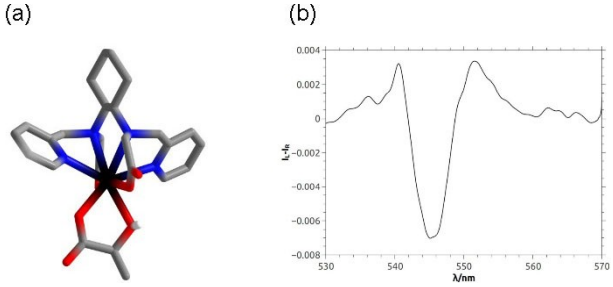

Figure 14. (a) Minimum energy structures of the [Y(*S,S*-bpcd)L-lactate] complex in the case of *trans*-Npy, Npy isomer. (b) CPL spectrum of [Tb(*rac*-bpcd)]$^+$ (5 mM) in a commercial Ringer's lactate solution, upon excitation at 265 nm. Adapted from Ref. [79] with permission (2018) from the Centre National de la Recherche Scientifique (CNRS) and the Royal Society of Chemistry

for the formation of the adduct is around 6 [5.94 for Tb(bpcd)$^+$ and 5.76 for Eu(bpcd)$^+$, evaluated through fluorimetric titration.[63] By means of DFT calculations, the structure of the 1:2 adduct was shown to present a bidentate HCO_3^- in the 1:1 adduct and two monodentate units in the 1:2 one (Figure 15).

The unprecedented affinity of the positively charged Eu(bpcd)$^+$ and Tb(bpcd)$^+$ complexes seems connected with a combination of three factors: small steric hindrance at the metal ion, positive charge and the relatively low coordination number of the ligand (CN = 6). In addition, the Eu(III) pyridine-based complex shows the best sensitivity of the optical response towards HCO_3^- in the concentration range related to metabolic acidosis (0-10 mM). A similar stoichiometry was found for the Eu(bQcd)$^+$/HCO_3^- adduct, but with a lower logK (4.62).[63]

2.2.3.3. Bovine Serum Albumin (BSA)

The interaction among bovine serum albumin (BSA) and two DACH-based Eu(III) complexes was studied by means of several experimental techniques.[53] Interestingly, we demonstrated that the nature of this interaction is strongly affected by the type of the involved heteroaromatic antenna in the Eu(III) complexes. In fact, when the *iso*quinoline ring is present, the corresponding complex [Eu(b*iso*Qcd)]$^+$ interacts with the protein into the superficial area containing the tryptophan residue 134 (Trp134). The Eu(III) ion is directly involved in the interaction as one coordinating water molecules is replaced by a glutamate side chain (E17) (Figure 16a).

This is in line with an increase of both the Eu(III) luminescence lifetime and luminescence intensity, upon titration of the complex with the protein. Conversely, the similar complex containing pyridine rings [Eu(bpcd)]$^+$ interacts more weakly with the protein [logK = 3.7 *vs.* 3.9 in the case of isoquinoline-based complex] and in a different superficial cavity, without losing the coordinated water molecules (Figure 16b). The different nature of the protein/complex interaction is marked by a different spectroscopic response of the complexes: in this case, no change in the Eu(III) luminescence lifetime and a decrease of the Eu(III) luminescence intensity are observed upon addition of BSA to the complex in aqueous solution. Unfortunately, as the CPL spectra of both complexes do not change significantly upon addition of the protein, this chiroptical technique is not helpful to sense BSA in aqueous solution.

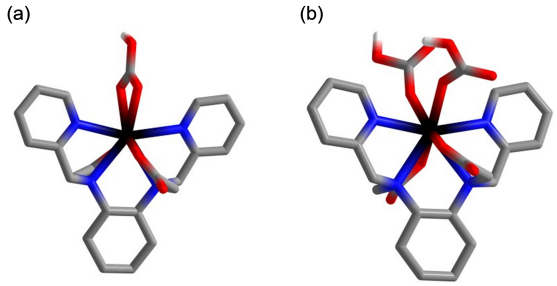

Figure 15. Minimum energy structures of (a) [Y(*trans*-O,O-bpcd)(HCO_3)] and (b) [Y(*trans*-O,O-bpcd)(HCO_3)$_2$]$^-$ which present the unusual *bis*-hydrogen carbonate coordination mode. Adapted from Ref. [63] with permission (2019) from the Royal Society of Chemistry

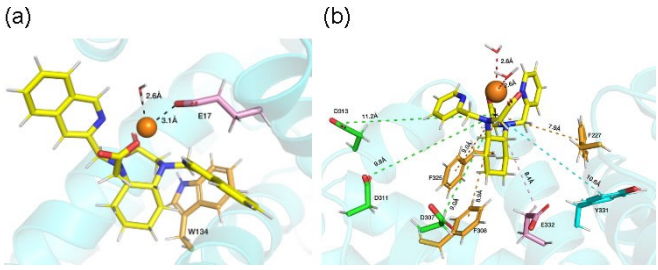

Figure 16. Snapshot of the interaction site of BSA with the [Y(b*iso*Qcd)(H_2O)]$^+$ (a) and [Eu(bpcd)(H_2O)$_2$]$^+$ (b) complexes. Adapted from Ref. [53] with permission, available at https://pubs.acs.org/doi/10.1021/acs.inorgchem.0c01663; further permissions related to the material excerpted should be directed to the ACS.

2.2.3.4. Citrate

To perform optical sensing experiments in complex matrix, such as interstitial extracellular fluids, the very good affinity of the Eu(bpcd)$^+$ and Tb(bpcd)$^+$ towards hydrogen carbonate appears promising and selectivity towards this molecule is expected in such a complex aqueous solution containing competitive analytes. Nevertheless, we had to face difficulties caused by the overlap between the excitation band of the bpcd-based complexes and the main absorption band of the proteins present in serum (BSA and HSA, λ_{max} = 290 nm overlaps with the absorption of the pyridine antenna; λ = 280 nm). Consequently, no efficient excitation of the optical probe is possible. A more convenient excitation wavelength, around 330 nm, can be used in the case of *iso*quinoline-based complexes, even though the steric hindrance at the metal ion should be slightly increased. As a consequence, the affinity towards HCO_3^- of Eu(b*iso*Qcd)$^+$ complex [logK = 4.6 for the [Eu(b*iso*Qcd)(HCO_3)$_2$]$^-$ adduct] is lower than that of Eu(bpcd)$^+$ [logK = 5.76]. Eu(b*iso*Qcd)$^+$ shows similar affinity for citrate and BSA [log K = 3.9(2) and 4.1(3), respectively.[52] Similar thermodynamic properties are found for the neutral counterpart Eu(*iso*QC3A) (Figure 9): log values of the binding constant with HCO_3^-, BSA and citrate are 3.4(1), 4.2(6) and 4.1(2), respectively. Apparently, on the basis of the affinity of the isoquinoline-based probes towards such analytes, no selective detection seems possible. On the contrary, a selective optical response towards citrate is recorded when a simulated interstitial extracellular fluid containing hydrogen carbonate, BSA, L-lactate, hydrogen phosphate and sulfate at their typical concentration, is considered. An increase of 23% of the luminescence intensity at 615 nm is recorded when the citrate concentration is raised up to 0.5 mM, in the case of Eu(b*iso*Qcd)$^+$ complex. A possible explanation for such optical selectivity should resides in the higher Eu(III) luminescence quantum yield of the citrate adducts, when compared with the adducts with BSA and hydrogen carbonate. Citrate is capable

to bind Eu(III) metal center by using its α-hydroxyl and α-carboxylate groups (Figure 17) in such a way that all the bound water molecules are removed and MPR process which is detrimental to luminescence efficiency, is quite reduced.

It is proposed that upon interaction with citrate, the Eu(III) ion is better protected than in the case of the other analytes, by the intrusion of water molecules (both in the inner and outer coordination spheres). To the best of our knowledge, our investigated Eu(III) complexes represent the first example of selective optical probes towards citrate in interstitial extracellular fluid-like matrix.

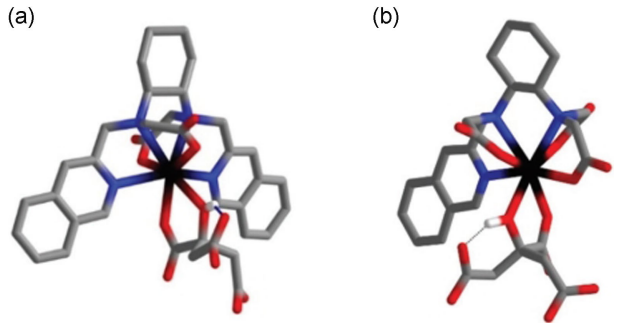

Figure 17. Minimum energy structures of (a) $[Y(bisoQcd)cit]^{2-}$ and (b) $[Y(isoQC3A)cit]^{3-}$ adducts; cit = citrate. *trans*-O,O isomers are considered.

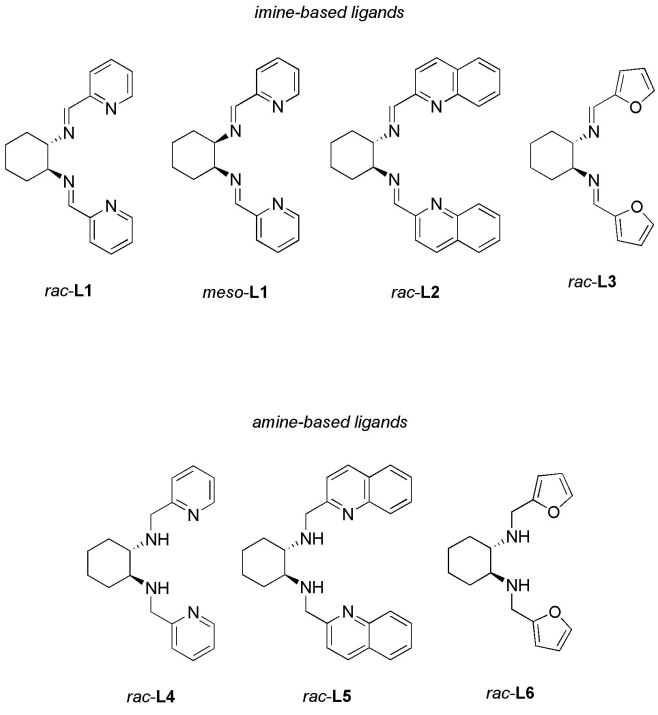

Figure 18. Structure of the molecules used as tetradentate ligands for Ln(III) discussed in this section.

2.3. Ln(III) Complexes Containing Pyridine, Quinoline and Furan-Based Tetradentate Ligands, Soluble in Organic Solvents

2.3.1. Thermodynamics and Structural Characterization in Acetonitrile

Tetradentate ligands containing pyridine, furan and quinoline chromophores (Figure 18) were synthesized by some of us.[80–82]

They differ mainly in the nature of the chromophoric fragment and degree of reduction of two C–N bonds (imine or amine). The chiral racemic DACH is generally used (Figure 18) although a different ligand stereochemistry was investigated in the case of **L1**, where the *cis* achiral isomer of DACH has been considered (Figure 1). A thermodynamic study performed in acetonitrile by means of UV/Vis spectroscopic titration reveals that in the case of *rac*-**L1**, complexes of different stability and stoichiometry are possible when different Eu(III) salt are used during the complexation.[83] In the case of trifluoromethanesulfonate (triflate) salt two complexes with 1:1 and 1:2, metal to ligand mole ratio and high stability constant [log K = 9.03 and 16.52, respectively] are detected, whilst in the case of nitrate salt only one species (1:1) is observed with a lower stability constant [logK = 6.87]. This evidence agrees with the different coordination ability of nitrate and triflate, the former being more coordinating in acetonitrile solution.

Similar conclusions can be drawn when the racemic **L3**, **L4** and **L6** ligands are considered (Table 6).

Despite the same tetradentate coordination mode of the ligands, the different stability of the related complexes can be rationalized considering the following aspects: *i*) the lower coordination ability of furan if compared with pyridine, *ii*) the higher solvation of the amine ligands and their complexes with respect to imine ones. Furthermore, *iii*) the less preorganized amines pay a higher energy cost in order to reach the conformation suitable for binding the Eu(III) cation.[81]

2.3.2. Luminescence and Optical Sensing Properties Towards Anions in Acetonitrile

The Eu(III) emission spectra of the triflate and nitrate complexes dissolved in acetonitrile solution shown a dominant band corresponding to the $^5D_0 \rightarrow {}^7F_2$ transition, as expected. In fact,

Table 6. Overall stability constants (log β_j, j = 1, 2) for the reaction Eu + jL ⇄ EuLj (charges omitted, L = L1, L3, L4 and L6 in Figure 13) of the triflate and nitrate complexes in acetonitrile.[81]

Salt		*rac*-**L1**	*rac*-**L3**	*rac*-**L4**	*rac*-**L6**
$Eu(NO_3)_3$	$\log\beta_1$	6.86	4.8	6.3	5.0
$Eu(CF_3SO_3)_3$	$\log\beta_1$	9.03	8.5	7.5	5.45
	$\log\beta_2$	16.52	13.5	14.5	10.04

the local Eu(III) symmetry must deviate from the inversion symmetry when chiral complexes are studied and forced electric dipole transitions become dominant. Interestingly, for the triflate and nitrate complexes of the imine-based molecules, we observed different asymmetry ratio[84] that can be effectively exploited in sensing experiment of nitrate ion in solution. The sensitivity of the Eu(III) emission intensity around 620 nm towards the presence of nitrate is tuned by the nature of the heteroaromatic ring; the less donating furan confers the best sensitivity (Figure 19).[81] Unfortunately, this aromatic moiety is not a good sensitizer of the Eu(III) luminescence and only the direct Eu(III) excitation around 395 nm is possible.

Other crucial characteristics, which significantly affect the sensitivity of the Eu(III) optical response towards nitrate are represented by the metal to ligand mole ratio of the starting triflate complex, which can be 1:1 or 1:2. Also, the concentration of the complexes plays an important role, as the number of anions (triflate or nitrate) bound to the metal ion is a function of the concentration of the species and strongly affect the Eu(III) luminescence features. On the contrary, although the stereochemistry of the ligands (*rac*-**L1** or *meso*-**L1**; figure 13) does not strongly affect the luminescence sensing towards nitrate,[85] it plays an important role in the optical sensing oft he bromide anion. Only *meso*-**L1** is capable to promote the Eu(III) luminescence sensing towards this ion.[50]

Interestingly, aqueous solutions of the Eu(*rac*-**L4**)$_2$(CF_3SO_3)$_3$ complex and copper nanoparticles, both embedded into amorphous films of polyvinyl alcohol with hydroxyethyl cellulose, have been prepared. The interaction of the complex with surface plasmons of the copper nanoparticles gives rise to an increase of the Eu(III) luminescence intensity by 300 %.[86]

As for the CPL activity of the investigated compounds, the Eu(III) nitrate complexes of enantiopure **L1** and **L2** show very low g_{Em} (around 10^{-2}–10^{-3}) both in solid and in acetonitrile solution. On the contrary the 1:1 triflate complexes present interesting values of g_{Em} only for the **L2** ligand; in acetonitrile at 592 nm its value is 0.2, while is 0.15 around 611 nm.

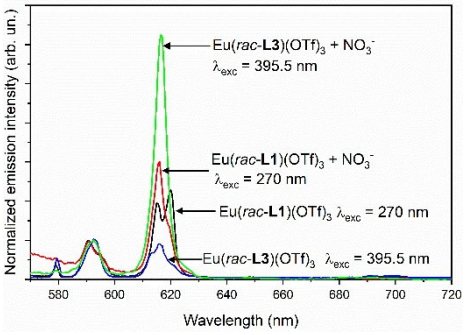

Figure 19. Evolution of the Eu(III) luminescence emission spectra upon addition of the nitrate anion, for complexes Eu(*rac*-**L1**)$(OTf)_3$ and Eu(*rac*-**L3**)$(OTf)_3$. [Eu(*rac*-**L1**)$(OTf)_3$] = [Eu(*rac*-**L3**)$(OTf)_3$] = 1 mmol dm^{-3}; [NO_3^-] = 4 mmol dm^{-3}. OTf = CF_3SO_3. Adapted from Ref. [81] with permission (2015) from the Royal Society of Chemistry.

2.3.3. Luminescence Properties in the Solid State

The nitrate complexes Ln(*rac*-**L1**)$(NO_3)_3$, Ln(*rac*-**L2**)$(NO_3)_3$, Ln(*rac*-**L4**)$(NO_3)_3$ and Ln(*rac*-**L5**)$(NO_3)_3$ in the solid state exhibit, upon ligand excitation, interesting spectroscopic properties. In particular, whilst the free ligands are not emissive, these complexes exhibit intra-ligand (IL) fluorescence in the blue visible region (400–450 nm) when Ln=La, Gd and Lu. In the case of **L1** and **L2** imine-based ligands the fluorescence seems promoted by the stiffness of the ligand upon complexation, whilst in the case of amine-based **L4** and **L5** the chelation enhanced fluorescence (CHEF) effect could be dominant.[82,87] Surprisingly, Gd(*rac*-**L1**)$(NO_3)_3$ and, to a less extent, also Gd(*rac*-**L5**)$(NO_3)_3$ and Lu(*rac*-**L5**)$(NO_3)_3$ complexes, show phosphorescence emission at room temperature around 600 nm [Gd(*rac*-**L1**)$(NO_3)_3$] and 530 nm [Gd(*rac*-**L5**)$(NO_3)_3$ and Lu(*rac*-**L5**)$(NO_3)_3$]. This emission should be promoted by the "paramagnetic effect" and/or "heavy-atom effect" well discussed in the Ref. [88]. Furthermore, all these ligands can sensitize the Eu(III) luminescence, whilst the Tb(III) luminescence can be stimulated only by pyridine-based ligands (*rac*-**L1** and *rac*-**L4**), even though a metal to ligand back energy transfer is responsible for a significant decrease of the $^5D_4$ Tb(III) luminescence lifetime, in the case of Tb(*rac*-**L1**)$(NO_3)_3$. This is mainly due to the position of the barycenter of singlet and triplet excited states of the ligands.[89] Both *rac*-**L4** and *rac*-**L5** ligands present triplet states whose energy is optimal to sensitize Eu(III) luminescence [almost 2000 cm^{-1} above the energy of $^5D_0$ level of Eu(III)]. Upon application of a hydrostatic pressure, a decrease of the energy of the ligands electronic levels is responsible for the worsening of the ligand to metal energy transfer. Only in the case of the amine-based (*rac*-**L4** and *rac*-**L5**) Eu(III) complexes, a back energy transfer is not involved in the deterioration of the emission intensity.

2.3.3.1. Luminescence Sensing Towards Acetonitrile Vapor

The evolution over the time of the Eu(III) $^5D_0 \rightarrow {}^7F_2$ luminescence emission band upon exposure to acetonitrile vapor of the [Eu(*meso*-**L1**)$(NO_3)_3$] complex in the solid state, is reported (Figure 20).[90]

Interestingly, at 293 K, upon an acetonitrile vapor pressure of ~$0.1 \cdot 10^5$ Pa, the crystal lattice of the complex is capable of absorbing and desorbing selectively acetonitrile molecules. This partially reversible process affects both crystal lattice parameters and the Eu(III) luminescence spectroscopy of [Eu(*meso*-**L1**)$(NO_3)_3$].

2.3.4. Chiroptical Properties of Heteroleptic Complexes Containing the 2-Thenoyltrifluoroacetyl-acetonate (tta) Ligand

The enantiopure [Eu**L1**(tta)$_2$(H_2O)](CF_3SO_3) complex was prepared and structurally characterized by means of single crystal X-ray diffraction (Figure 21).[65]

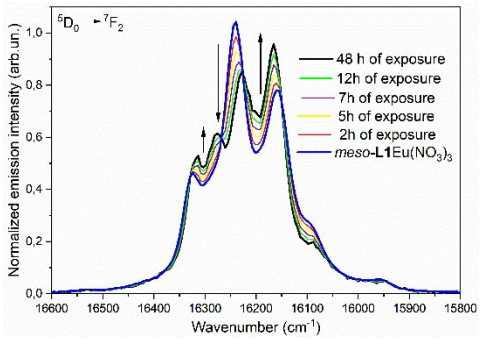

Figure 20. Evolution over the time of the Eu(III) $^5D_0 \rightarrow {}^7F_2$ luminescence emission band of the [Eu(*meso*-**L1**)$(NO_3)_3$] complex upon exposure to acetonitrile vapor. Excitation was at 273 nm. Adapted with permission from Ref. [90]. Copyright (2021) Elsevier.

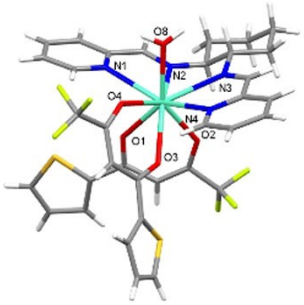

Figure 21. Crystal structure of [Eu**L1**$(tta)_2(H_2O)]$ CF_3SO_3. Triflate anion is omitted for sake of clarity. Adapted with permission from Ref. [65]. Copyright (2018) American Chemical Society.

Despite the presence of one water molecule bound to Eu(III), the intrinsic quantum yield is around 40% in acetonitrile and rises to 52% in methanol, where the water molecule is replaced by CH_3OH. Also in the solid state, **L1** and tta molecules can efficiently harvest and transfer to Eu(III) the UV light absorbed in the 250–400 nm range and the forced electric-dipole $^5D_0 \rightarrow {}^7F_2$ emission band dominates the Eu(III) emission spectra. The light

emitted by the enantiopure complex shows a sizable degree of polarization with a value of g_{Em} equal to 0.2 in methanol solution and 0.1 in solid. In parallel, also the analog Sm(III) complex was investigated.[91] The tta molecule is a good sensitizing ligand also for Sm(III) luminescence and a good value of g_{Em} was recorded (0.03 both in methanol and acetonitrile). Thanks to all these features, these compounds can be considered promising candidates as red-orange phosphors in CP-OLED devices. Worthy of note is the dependence of the CPL signature of the complexes from a concurrent effect of the solvent and counterion. This particularly applies to europium (III) complexes where for both triflate and nitrate complexes, the CPL spectra in acetonitrile can be described as a weighed linear combination of the CPL spectra in dichloromethane and methanol[91] Surprisingly, these CPL spectra show nearly opposite signatures although the ligand stereochemistry is the same (Figure 22).

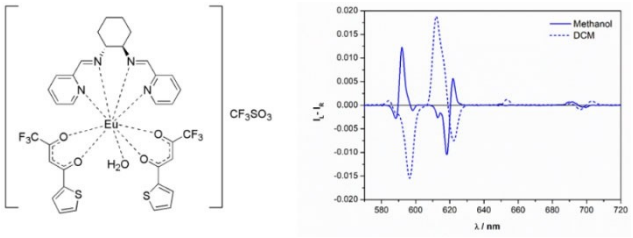

Figure 22. Nearly opposite CPL signature of the (R,R)-[Eu**L1**$(tta)_2(H_2O)]CF_3SO_3$ complex when dissolved in two different solvents such as methanol and dichloromethane. Adapted from Ref. [91] with permission, available at https://pubs.acs.org/doi/10.1021/acs.inorgchem.0c00280; further permissions related to the material excerpted should be directed to the ACS.

The complexity of the species in solution has been documented by DFT calculations. Equilibria interconverting different species where the counterions is bound (in dichloromethane) or not (in methanol) to the metal ion, occur. In addition, the presence of isomeric species differing by the relative orientation of the tta ligands is also possible. DFT calculations underline different M–N bond lengths in the different species. This evidence should have a crucial role in the definition of the CPL activity. On the contrary, no significant solvent effect is observed in the UV/Vis and ECD spectra and only negligible changes are detected in the luminescence spectra.

3. Conclusions and Perspectives

In this minireview, we discuss the use of the chiral *trans*-1,2-diaminocyclohexane as a backbone of a multitude of ligands and the related metal complexes, which find important applications in several fields. In particular, lanthanide-based complexes show very interesting thermodynamic and spectroscopic properties. As discussed in the text, the rigidifying effect of the cyclohexane unit can improve the stability and the kinetic inertness of the chelate molecules. This characteristic is crucial when in vivo applications are foreseen, especially in the biomedical field. Furthermore, the chirality of DACH, combined with suitable chromophores like pyridine rings, gives rise to an unprecedented CPL activity (i.e. unusually high g_{Em} values stemming from Tb(III) and Eu(III) transitions which normally do not exhibit strong CPL signals). The rigidity of the cyclohexane ring is also responsible for the higher values of the emission quantum yield, when within the ligand, DACH is combined with 2-hydroxyisophthalamide (IAM) antenna. In the case of the related Tb(III) complex no solvent molecules are present in the in the inner coordination sphere of the metal ion, so that a high value of the quantum yield is ensured.

Ligands where DACH is combined with other chromophores, such as pyridine, quinoline and *iso*quinoline rings produces highly stable and water soluble Eu(III) and Tb(III) complexes. Their optical and chiroptical properties are reviewed, also in the direction of potential applications as probes for the detection of important bio-analytes. Precursors of these ligands, soluble in organic solvent, form Eu(III) complexes

capable to selectively detect inorganic anions in acetonitrile solution and acetonitrile vapors in the case of solid sample of one complex of these family. An heteroleptic Eu(III) complex containing pyridine-based and tta ligands shows a very uncommon dependence of the CPL signature on a concurrent effect of the solvent and counterion.

In conclusion, it can be said that in all the applications involving chirality (i.e. catalysis, chiral discrimination, pharmaceutics, supramolecular chemistry, molecular recognition and (chiro)optics) DACH seems to play a leading role and in our opinion, it still has a lot to give to scientists working in this very fascinating field.

Acknowledgements

The authors thank the Italian Ministry of University and Research for the received funds (PRIN (Progetti di Ricerca di Rilevante Interesse Nazionale) project "CHIRALAB", Grant No. 20172M3K5N). FP, CN and MB gratefully also thank the Facility "Centro Piattaforme Tecnologiche" of the University of Verona for access to the Fluorolog 3 (Horiba-Jobin Yvon) spectrofluorometer. Funding from the University of Verona is gratefully acknowledged. Open Access Funding provided by Universita degli Studi di Verona within the CRUI-CARE Agreement.

Conflict of Interest

The authors declare no conflict of interest.

Keywords: circularly polarized luminescence · chiroptical properties · lanthanides · optical sensing

[1] H.-J. Schanz, M. A. Linseis, D. G. Gilheany, *Tetrahedron: Asymmetry* **2003**, *14*, 2763–2769.
[2] Y. Zhang, X. Zhang, S. Ma, *Nat. Commun.* **2021**, *12:2416*, 1–12.
[3] M. Serra, E. Bernardi, G. Marrubini, E. De Lorenzi, L. Colombo, *Eur. J. Org. Chem.* **2019**, *2019*, 732–741.
[4] R. T. Endean, L. Rasu, S. H. Bergens, *ACS Catal.* **2019**, *9*, 6111–6117.
[5] Y. N. Belokon, P. Carta, A. V. Gutnov, V. Maleev, M. A. Moskalenko, L. V. Yashkina, N. S. Ikonnikov, N. V. Voskoboev, V. N. Khrustalev, M. North, *Helv. Chim. Acta* **2002**, *85*, 3301–3312.
[6] T. R. J. Achard, L. A. Clutterbuck, M. North, *Synlett* **2005**, 1828–1847.
[7] D. Xiong, M. Wu, S. Wang, F. Li, C. Xia, W. Sun, *Tetrahedron: Asymmetry* **2010**, *21*, 374–378.
[8] S. V. Samuelsen, C. Santilli, M. S. G. Ahlquist, R. Madsen, *Chem. Sci.* **2019**, *10*, 1150–1157.
[9] J. Chun, S. Kang, N. Kang, S. M. Lee, H. J. Kim, S. U. Son, *J. Mater. Chem. A* **2013**, *1*, 5517–5523.
[10] C. Freire, M. Nunes, C. Pereira, D. M. Fernandes, A. F. Peixoto, M. Rocha, *Coord. Chem. Rev.* **2019**, *394*, 104–134.
[11] D. T. Payne, M. K. Chahal, V. Březina, W. A. Webre, K. Ariga, F. D'Souza, J. Labuta, J. P. Hill, *Front. Chem.* **2020**, *14*, 28–40.
[12] X. Hua, A. von Zelewsky, *Inorg. Chem.* **2002**, *34*, 5791–5797.
[13] Zi–Bo Li, Jing Lin, Michal Sabat, Marilise Hyacinth, L. Pu, *J. Org. Chem.* **2007**, *72*, 4905–4916.
[14] Q. Liu, Q. Xia, Y. Xiong, B. S. Li, B. Z. Tang, *Macromolecules* **2020**, *53*, 6288–6298.
[15] P. Reine, A. M. Ortuño, I. F. A. Mariz, M. Ribagorda, J. M. Cuerva, A. G. Campaña, E. Maçôas, D. Miguel, *Front. Chem.* **2020**, *8*, 306.
[16] K. Kato, Y. Ichimaru, Y. Okuno, Y. Yamaguchi, W. Jin, M. Fujita, M. Otsuka, M. Imai, H. Kurosaki, *Bioorg. Med. Chem. Lett.* **2021**, *36*, 127834.
[17] F. Arnesano, A. Pannunzio, M. Coluccia, G. Natile, *Coord. Chem. Rev.* **2015**, *284*, 286–297.
[18] D. M. Fisher, P. J. Bednarski, R. Grünert, P. Turner, R. R. Fenton, J. R. Aldrich-Wright, *ChemMedChem* **2007**, *2*, 488–495.
[19] P. Zsabka, K. Van Hecke, L. Adriaensen, A. Wilden, G. Modolo, M. Verwerft, K. Binnemans, T. Cardinaels, *Solvent Extr. Ion Exch.* **2018**, *36*, 519–541.
[20] A. Wilden, F. Kreft, D. Schneider, Z. Paparigas, G. Modolo, G. J. Lumetta, A. V. Gelis, J. D. Law, A. Geist, *Appl. Sci.* **2020**, *10*, 7217.
[21] J. Gregoliński, T. Lis, M. Cyganik, J. Lisowski, *Inorg. Chem.* **2008**, *47*, 11527–11534.
[22] J. Gregoliński, R. Wieczorek, J. Lisowski, *Eur. J. Inorg. Chem.* **2011**, *2011*, 3717–3725.
[23] J. Lisowski, J. Mazurek, *Polyhedron* **2002**, *21*, 811–816.
[24] J. Gregoliński, A. Kochel, J. Lisowski, *Polyhedron* **2006**, *25*, 2745–2754.
[25] A. Jana, S. Majumder, L. Carrella, M. Nayak, T. Weyhermueller, S. Dutta, D. Schollmeyer, E. Rentschler, R. Koner, S. Mohanta, *Inorg. Chem.* **2010**, *49*, 9012–9025.
[26] R. Peacock, in *Rare Earths SE – 3*, Springer Berlin Heidelberg, **1975**, pp. 83–122.
[27] J. C. G. Bünzli, S. V. Eliseeva, *Chem. Sci.* **2013**, *4*, 1939–1949.
[28] L. Ungur, in *Lanthanide-Based Multifunct. Mater.* (Eds.: P. Martin-Ramos, M. Ramos-Silva), Elsevier, Amsterdam, **2018**, pp. 1–58.
[29] C. M. Dodson, R. Zia, *Phys. Rev. B: Condens. Matter Mater. Phys.* **2012**, *86*, 125102.
[30] M. J. Weber, *Phys. Rev.* **1968**, *171*, 283–291.
[31] J. M. F. Van Dijk, M. F. H. Schuurmans, *J. Chem. Phys.* **1983**, *78*, 5317–5323.
[32] H. U. Güdel, M. Pollnau, *J. Alloys Compd.* **2000**, *303–304*, 307–315.
[33] E. Kreidt, C. Kruck, M. Seitz, in *Handb. Phys. Chem. Rare Earths*, Elsevier B. V., **2018**, pp. 35–79.
[34] L. Armelao, S. Quici, F. Barigelletti, G. Accorsi, G. Bottaro, M. Cavazzini, E. Tondello, *Coord. Chem. Rev.* **2010**, *254*, 487–505.
[35] E. G. Moore, A. P. S. Samuel, K. N. Raymond, *Acc. Chem. Res.* **2009**, *42*, 542–552.
[36] F. S. Richardson, *Inorg. Chem.* **1980**, *19*, 2806–2812.
[37] L. Arrico, L. Di Bari, in *Springer Ser. Fluoresc. (Methods Appl.*, Springer, Cham, **2021**, pp. 1–35.
[38] P. Di Bernardo, A. Melchior, M. Tolazzi, P. L. Zanonato, *Coord. Chem. Rev.* **2012**, *256*, 328–351.
[39] A. C. Mendonça, A. F. Martins, A. Melchior, S. M. Marques, S. Chaves, S. Villette, S. Petoud, P. L. Zanonato, M. Tolazzi, C. S. Bonnet, É. Tóth, P. Di Bernardo, C. F. G. C. Geraldes, M. A. A. Santos, *Dalton Trans.* **2013**, *42*, 6046–57.
[40] P. Caravan, J. J. Ellison, T. J. McMurry, R. B. Lauffer, *Chem. Rev.* **1999**, *99*, 2293–2352.
[41] R. G. Pearson, *J. Am. Chem. Soc.* **1963**, *85*, 3533–3539.
[42] A. E. Martell, R. D. Hancock, R. J. Motekaitis, *Coord. Chem. Rev.* **1994**, *133*, 39–65.
[43] A. E. Martell, R. J. Motekaitis, *Determination and Use of Stability Constants*, Wiley, **1992**.
[44] F. Endrizzi, P. Di Bernardo, P. L. Zanonato, F. Tisato, M. Porchia, A. A. Isse, A. Melchior, M. Tolazzi, *Dalton Trans.* **2017**, *46*, 1455–1466.
[45] S. Gràcia Lanas, M. Valiente, E. Aneggi, A. Trovarelli, M. Tolazzi, A. Melchior, *RSC Adv.* **2016**, *6*, 42288–42296.
[46] P. Di Bernardo, P. L. L. Zanonato, A. Bismondo, A. Melchior, M. Tolazzi, *Dalton Trans.* **2009**, 4236–4244.
[47] P. Di Bernardo, P. L. Zanonato, A. Melchior, R. Portanova, M. Tolazzi, G. R. Choppin, Z. Wang, *Inorg. Chem.* **2008**, *47*, 1155–1164.
[48] P. Luigi Zanonato, P. Di Bernardo, A. Melchior, M. Busato, M. Tolazzi, *Inorg. Chim. Acta* **2020**, *503*, 119392.
[49] S. Del Piero, A. Melchior, P. Polese, R. Portanova, M. Tolazzi, *Eur. J. Inorg. Chem.* **2006**, *2006*, 304–314.
[50] F. Piccinelli, M. Leonzio, M. Bettinelli, A. Melchior, G. Faura, M. Tolazzi, *Inorg. Chim. Acta* **2016**, *453*, 751–756.
[51] R. Credendino, Y. Minenkov, D. Liguori, F. Piemontesi, A. Melchior, G. Morini, M. Tolazzi, L. Cavallo, *Phys. Chem. Chem. Phys.* **2017**, *19*, 26996–27006.
[52] C. De Rosa, A. Melchior, M. Sanadar, M. Tolazzi, A. Duerkop, F. Piccinelli, *Dalton Trans.* **2021**, *50*, 4700–4712.
[53] C. De Rosa, A. Melchior, M. Sanadar, M. Tolazzi, A. Giorgetti, R. P. Ribeiro, C. Nardon, F. Piccinelli, *Inorg. Chem.* **2020**, *59*, 12564–12577.
[54] S. J. Butler, D. Parker, *Chem. Soc. Rev.* **2013**, *42*, 1652–1666.

[55] K. M. Ayers, N. D. Schley, G. Ung, *Inorg. Chem.* **2020**, *59*, 7657–7665.
[56] D. Schnable, K. Freedman, K. M. Ayers, N. D. Schley, M. Kol, G. Ung, *Inorg. Chem.* **2020**, *59*, 8498–8504.
[57] G. Tircso, M. Regueiro-Figueroa, V. Nagy, Z. Garda, T. Garai, F. K. Kàlmàn, D. Esteban-Gòmez, É. Tòth, C. Platas-Iglesias, *Chem. Eur. J.* **2016**, *22*, 896–901.
[58] A. P. S. Samuel, J. L. Lunkley, G. Muller, K. N. Raymond, *Eur. J. Inorg. Chem.* **2010**, *2010*, 3343–3347.
[59] M. Seitz, E. G. Moore, A. J. Ingram, G. Muller, K. N. Raymond, *J. Am. Chem. Soc.* **2007**, *129*, 15468–15470.
[60] P. Caravan, P. Mehrkhodavandi, C. Orvig, *Inorg. Chem.* **1997**, *36*, 1316–1321.
[61] M. Leonzio, A. Melchior, G. Faura, M. Tolazzi, F. Zinna, L. Di Bari, F. Piccinelli, *Inorg. Chem.* **2017**, *56*, 4413–4422.
[62] T. F. Gritmon, M. P. Goedken, G. R. Choppin, *J. Inorg. Nucl. Chem.* **1977**, *39*, 2021–2023.
[63] F. Piccinelli, C. De Rosa, A. Melchior, G. Faura, M. Tolazzi, M. Bettinelli, *Dalton Trans.* **2019**, *48*, 1202–1216.
[64] C. C. McLauchlan, J. Florián, D. S. Kissel, A. W. Herlinger, *Inorg. Chem.* **2017**, *56*, 3556–3567.
[65] M. Leonzio, M. Bettinelli, L. Arrico, M. Monari, L. Di Bari, F. Piccinelli, *Inorg. Chem.* **2018**, *57*, 10257–10264.
[66] K. L. Peterson, J. V. Dang, E. A. Weitz, C. Lewandowski, V. C. Pierre, *Inorg. Chem.* **2014**, *53*, 6013–6021.
[67] A. G. Weidmann, A. C. Komor, J. K. Barton, *Philos. Trans. R. Soc. London* **2013**, *371*, 20120117.
[68] C. A. Puckett, J. K. Barton, *J. Am. Chem. Soc.* **2007**, *129*, 46–47.
[69] A. S. Chauvin, F. Thomas, B. Song, C. D. B. Vandevyver, J. C. G. Bünzli, *Philos. Trans. R. Soc. London* **2013**, *371*, 20120295.
[70] E. J. New, A. Congreve, D. Parker, *Chem. Sci.* **2010**, *1*, 111–118.
[71] B. S. Murray, E. J. New, R. Pal, D. Parker, *Org. Biomol. Chem.* **2008**, *6*, 2085–2094.
[72] K. Binnemans, *Coord. Chem. Rev.* **2015**, *295*, 1–45.
[73] W. H. William De, D. R. Sudnick, *J. Am. Chem. Soc.* **1979**, *101*, 334–340.
[74] R. M. Supkowski, W. D. W. Horrocks, *Inorg. Chim. Acta* **2002**, *340*, 44–48.
[75] M. Albin, R. R. Whittle, W. D. W. Horrocks, *Inorg. Chem.* **1985**, *24*, 4591–4594.
[76] L. Arrico, L. Di Bari, F. Zinna, *Chem. A Eur. J.* **2021**, *27*, 2920–2934.
[77] A. Taniguchi, N. Hara, M. Shizuma, N. Tajima, M. Fujiki, Y. Imai, *Photochem. Photobiol. Sci.* **2019**, *18*, 2859–2864.
[78] R. Carr, N. H. Evans, D. Parker, *Chem. Soc. Rev.* **2012**, *41*, 7673–7686.
[79] M. Leonzio, A. Melchior, G. Faura, M. Tolazzi, M. Bettinelli, F. Zinna, L. Arrico, L. Di Bari, F. Piccinelli, *New J. Chem.* **2018**, *42*, 7931–7939.
[80] F. Piccinelli, A. Speghini, M. Monari, M. Bettinelli, *Inorg. Chim. Acta* **2012**, *385*, 65–72.
[81] F. Piccinelli, M. Bettinelli, A. Melchior, C. Grazioli, M. Tolazzi, *Dalton Trans.* **2015**, *44*, 182–192.
[82] M. Mihorianu, M. Leonzio, M. Monari, L. Ravotto, P. Ceroni, M. Bettinelli, F. Piccinelli, *ChemistrySelect* **2016**, *1*, 1996–2003.
[83] F. Piccinelli, A. Melchior, A. Speghini, M. Monari, M. Tolazzi, M. Bettinelli, *Polyhedron* **2013**, *57*, 30–38.
[84] E. W. J. L. Oomen, A. M. A. van Dongen, *J. Non-Cryst. Solids* **1989**, *111*, 205–213.
[85] F. Piccinelli, M. Leonzio, M. Bettinelli, M. Monari, C. Grazioli, A. Melchior, M. Tolazzi, *Dalton Trans.* **2016**, *45*, 3310–3318.
[86] R. Reisfeld, V. Levchenko, F. Piccinelli, M. Bettinelli, *J. Lumin.* **2016**, *170*, 820–824.
[87] M. Mihorianu, M. Leonzio, M. Bettinelli, F. Piccinelli, *Inorg. Chim. Acta* **2015**, *438*, 10–13.
[88] S. Tobita, M. Arakawa, I. Tanaka, *J. Phys. Chem.* **1985**, *89*, 5649–5654.
[89] F. Piccinelli, C. De Rosa, A. Lazarowska, S. Mahlik, M. Grinberg, T. Nakanishi, S. Omagari, M. Bettinelli, *Inorg. Chim. Acta* **2020**, *499*, 119179.
[90] F. Piccinelli, V. Paterlini, M. Monari, M. Bettinelli, *J. Rare Earth* **2020**, *38*, 571–576.
[91] L. Arrico, C. De Rosa, L. Di Bari, A. Melchior, F. Piccinelli, *Inorg. Chem.* **2020**, *59*, 5050–5062.

Manuscript received: July 7, 2021
Revised manuscript received: August 9, 2021
Accepted manuscript online: August 12, 2021
Version of record online: September 12, 2021